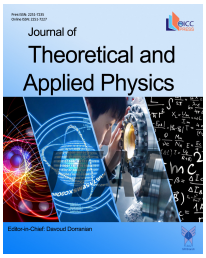

Volume 18, Issue 1, 182411 (1-6)

Journal of Theoretical and Applied Physics (JTAP)

https://doi.org/10.57647/j.jtap.2024.1801.11

Electric and magnetic dipole moments in super cell dielectric meta-surface

Noora Aziz Alweiy, Nizar Salim Shnan*, Jinan Ali Abd

Department of Laser Physics, College of Science for Women, University of Babylon, Babylon, Iraq.

***Corresponding authors**:nizarflifl@yahoo.com

ORIGINAL RESEARCH

Received:
22 Aug. 2023
Revised:
18 November 2023
Accepted:
10 December 2023
Published online:
10 January 2024

Abstract:

Two dimensional all dielectric grating metamaterial based on polydimethylsiloxane and TiO_2 materials were prepared via sputtering method in two different configurations as PDMS/TiO_2 (50 nm)) and 2D grating (etalon) TiO_2 (50 nm)/PDMS/TiO_2 (50 nm). As it was measured by a charged coupled device (CCD) camera, the hotspots confirm four points symmetry of the structure and also the refractive index falls in the negative part to show meta state. In addition, the absorption spectra show the clear separation between electric dipole (ED) and Magnetic dipoles (MD) by enhancing the incidence angle onto the sample. We noted the gradual increase in the angle begins to appear and became more noticeable from 52^o to 60^o and the reason for this separation at these angles may be the fall of the beam at an oblique angle, and it is clear that inclination at an oblique angle leads to a more pronounced metamaterial behavior.

Keywords: Electric dipole; Magnetic dipole; Meta-surface

1. Introduction

Metamaterials have opened new insights with potential applications in optical filters, medical devices, remote activation applications, intelligent energy management, infrastructure monitoring, solar and laser sensor detection [1–7]. In all-dielectric metasurfaces, nanoparticles cause diffractive scattering of the incident light, leading to the propagation of lattice surface modes (LSMs) within the structure. These LSMs, such as LSPRs in plasmonic nanostructures, have the ability to interfere with the localized excitations of each individual nanoparticle. As a result, the coupled scattering resonance is observed, leading to the narrowing of the reflection or transmission spectrum width of the all-dielectric structure. All-dielectric metasurfaces with high refractive index can also facilitate Mie scattering resonances, leading to the appearance of electric dipole (ED) and magnetic dipole (MD) resonant modes, and can enhance the optical field intensity by adjusting the incident wavelength to the resonance wavelength. Therefore, high-index all-dielectric nanostructures have become promising elements in modern nanophotonic systems due to low loss and tunable optical properties and offer potential applications in various fields such as lasing [8, 9], biosensing [10, 11], nonlinear optics [12], and structural color and color display [13].

Given the fact that all of the structures go to miniaturization and also flexible ones, the design and fabrication of new all-dielectric and flexible structures is mandatory for lab on a chip application. Thus, in this report, we fabricate and investigate the main physical reason of modes in the optical response by the aid of ED and MD within specific angles of incidence with the aid of optical refractometry and also Numerical simulator respectively.

2. Experimental part

The nanoimprint lithography approach has been used successfully to fabricate 2D metasurface grating. A Schematic array of the sample preparation is shown in Fig. 1a. Two different 2D charge-coupled devices (CCDs) were detached from a camera for this purpose, and these CCD stamps were then adhered to a glass substrate with a two-sided adhesive and enclosed in a plexiglass frame. The next step was to fill the frame with a sufficient amount of material that was roughly 1.4 mm thick after weighing the polydimethylsiloxane (PDMS) and the curing agent (1:10) and mixing them for 5 minutes [13–15]. For degassing, the sample was placed in a vacuum chamber for 15 min. This step was

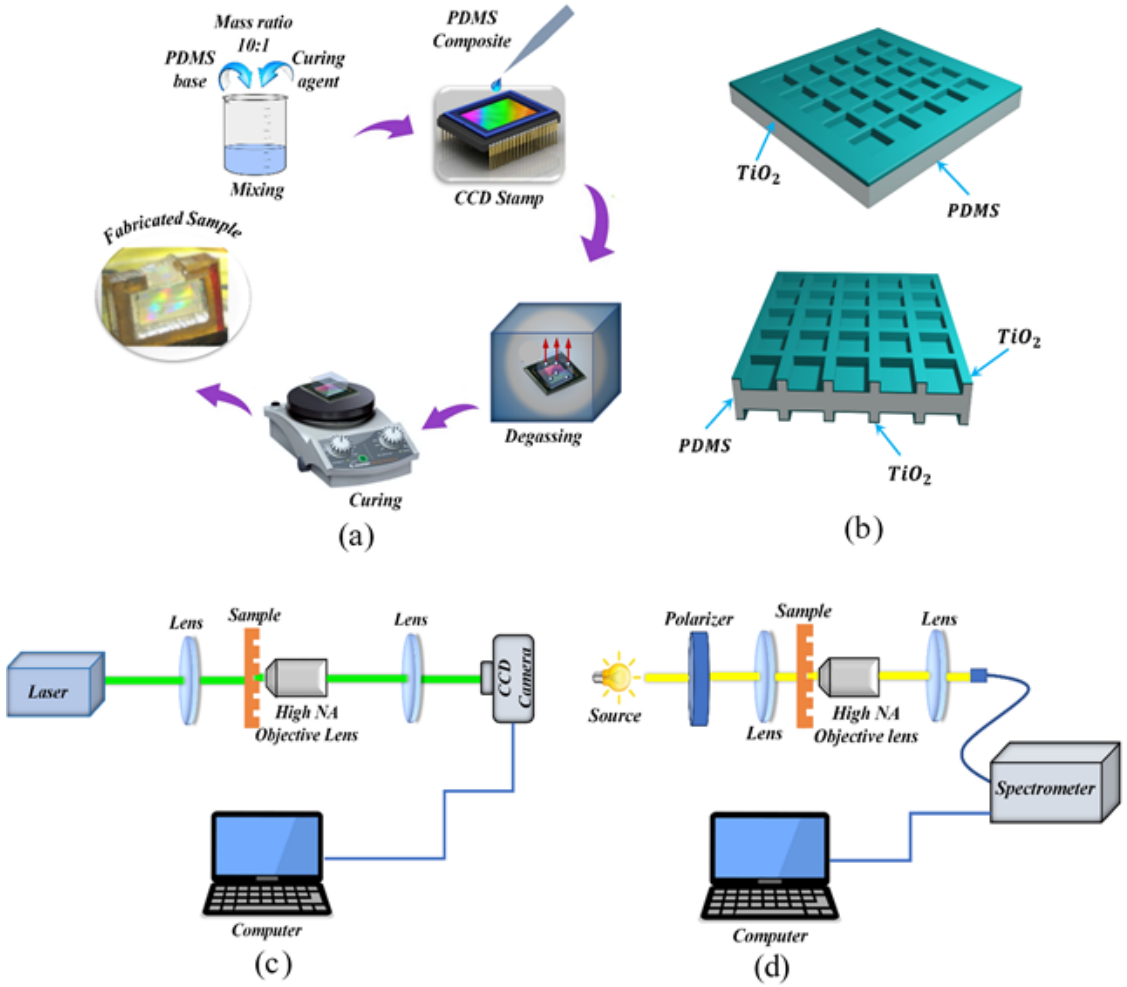

Figure 1. (a) Schematic diagram of the sample preparation steps, (b) first and second samples illustrations as one side 2D grating (PDMS/TiO_2(50nm)) and two-sided 2D grating (etalon) (TiO_2(50nm)/PDMS/TiO_2(50nm), (c) and (d) Experimental setup of samples' characterization by ccd camera and spectrometer.

carried out to remove air bubbles that formed during mixing. Afterward, the sample was cured at temperatures between 50^o and 100^o degrees for 1 hour using a hot plate. CCD stamps could be removed after roughly a day, provided the material has dried out, the resultant 2D surface was then coated with 100 nm of TiO_2 using a sputtering device. It should be mentioned that the radio frequency (RF) sputtering deposition of TiO_2 thin film was performed under the process conditions as follows: RF power of 70 W, chamber pressure of 0.004 mbar, Ar gas, thickness of 50 nm, and substrate rotation speed of 28 rpm.

The aforementioned procedures were carried out on two CCDs using two different types of unit cells. Thus, using two different types of unit cells, we created two samples of all-dielectric metasurfaces. The first sample as One-sided 2D grating (PDMS/TiO_2(50nm)), was from a two-dimensional single grating (PDMS/TiO_2(50nm)) structure. This sample consisted of a periodic two-dimensional square array onto the PDMS substrate covered with a thin layer of TiO_2 as displayed in Fig. 1b. In addition, the second sample as two-sides 2D grating (etalon) (TiO_2(50nm)/PDMS/TiO_2(50nm), consisted of a two-dimensional square periodic matrix, based on PDMS, covered with a thin layer of TiO_2 on both surfaces as shown in Fig. 1b.

A schematic array of the optical imaging and spectroscopy experimental setups is shown in Figs. 1c and d, respectively. In the optical imaging arrangement, the green laser beam is illuminated the sample, and the transmitted light is collected using a high numerical aperture (NA) objective lens. Finally transmitted light is focused onto a CCD camera using a lens (Fig. 1c). In this manner, the optical excitation and imaging of the sample can be performed.

On the other hand, the broadband halogen lamp was utilized as a light source in the spectroscopy experimental setup (Fig. 1d). The polarization of the light is controlled by a polarizer and the light with a certain polarization (s- or p-polarization) is focused on the sample. Afterward, the transmitted light is collected by the high NA objective lens and coupled to the spectrometer (Fig. 1d).

3. Results and discussion

As the first stage, the samples were examined by the X-ray diffraction techniques (XRD) to obtain the crystalline

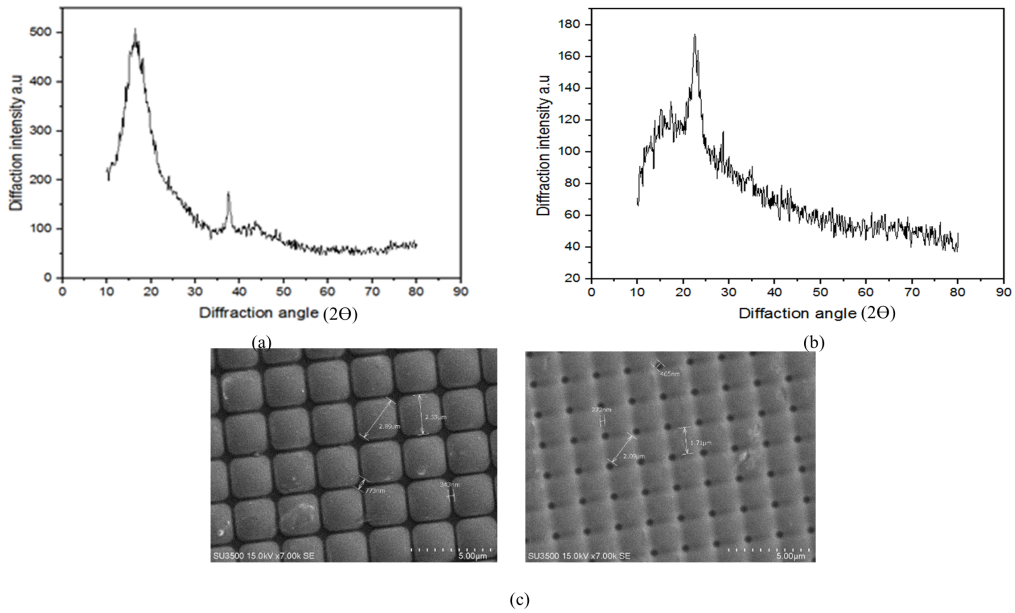

Figure 2. X-ray diffraction pattern of (a) S1, one-side 2D grating (PDMS/TiO_2 (50nm)), (b) S2, two-sided 2D grating (etalon) (TiO_2 (50nm)/PDMS/TiO_2 (50nm) and (c) SEM image of two-sided 2D grating (etalon) (TiO_2 (50nm)/PDMS/TiO_2 (50nm).

structure of them. Fig. 2 indicates that both samples as one sided, S1, and etalon, S2, have polycrystalline structure of metastable phase of β-TiO_2 according to the (JCPDS card No. 46-1238).

For S1 film, the notable preferred orientations are along (200), (401), and (020) planes at (2θ= 15.880°, 37.240°, and 48.080°) respectively. In addition, the notable preferred orientations of S2 are along (201), (002), and (310) planes at (2θ= 23.18°, 28.35°, and 33.68°) respectively. The patterns reveal disappearance of the notable orientations of S1 and appearance of different notable orientations in S_2. This behavior may be due to the layer-by-layer growth and recrystallization process corresponding to the preparation method of S1 in one- dimension and S2 in two dimensions. The evaluated data from XRD patterns have been reported in Table 1. The crystallite sizes (D) of the samples have been calculated using the evaluated data of XRD patterns by Scherrer formula;

$$D = \frac{0.9\lambda}{\beta \cos\theta} \tag{1}$$

where β is the full width at half maximum (FWHM), denotes the diffraction angle, and shows the incoming Cu-K_α radiation wavelength (1.5406 nm). The values for crystallite sizes show that the S1 and S2 nanocrystal films are present, as listed in Table 1. In addition, the crystalline nature of nanostructured films can be determined by many structural parameters such as dislocations density (δ) and strain (ε), which are calculated by equations 2 and 3 [14]:

$$\delta = \frac{1}{D^2} \tag{2}$$

$$\varepsilon = \frac{\beta \cos\theta}{4} \tag{3}$$

The structural parameters values of the preferred direction of S1 and S2 nanostructured films have been tabulated in Table 2. The low values of δ and ε indicate high quality and abundance of crystalline with low deformations in the films structure. One can see that, the particles have dimensions 2.7 to 3.04 nm and 2.53 to 2.89 nm and distance between the particles is 227 to 979 nm for S1 and S2 respectively.

For the second stage, pictures were captured using the CCD camera for the prepared samples, as well as the spectra were measured for the same samples using a spectrometer, with the results being presented in figure 3.

We notice through the results that the intensity is high in

Table 1. The extracted data from XRD.

Samples	(*hkl*)	2θ (°)	cos θ	β(°)	D (nm)
S1	(200)	15.88	0.990	3.96	2.02
	(401)	37.24	0.947	1.03	8.14
	(020)	48.08	0.913	3.96	2.19
S2	(201)	23.18	0.979	2.82	2.87
	(002)	28.35	0.969	1.6	5.12
	(310)	33.68	0.957	3.37	2.46

Table 2. Parameters of the structure of nanofilms.

Sample	Preferred orientation	D (nm)	δ (1/nm^2)	ε
S1	(200)	2.02	0.243	0.017
S2	(201)	2.87	0.120	0.012

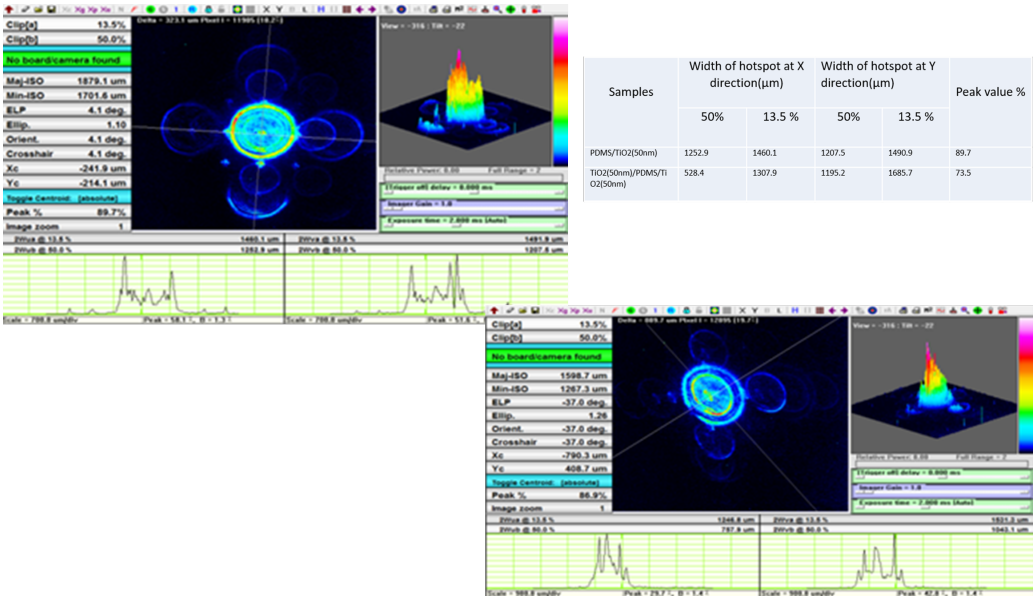

Samples	Width of hotspot at X direction(μm)		Width of hotspot at Y direction(μm)		Peak value %
	50%	13.5 %	50%	13.5 %	
PDMS/TIO2(50nm)	1252.9	1460.1	1207.5	1490.9	89.7
TIO2(50nm)/PDMS/TIO2(50nm)	528.4	1307.9	1195.2	1685.7	73.5

Figure 3. CCD image of the (a) S1, one-side 2Dgrating (PDMS/TiO_2 (50nm)) and (b)S2, two-sided 2D grating (etalon) (TiO_2 (50nm)/PDMS/TiO_2 (50nm) and Table which shows characteristics the hotspot of two samples.

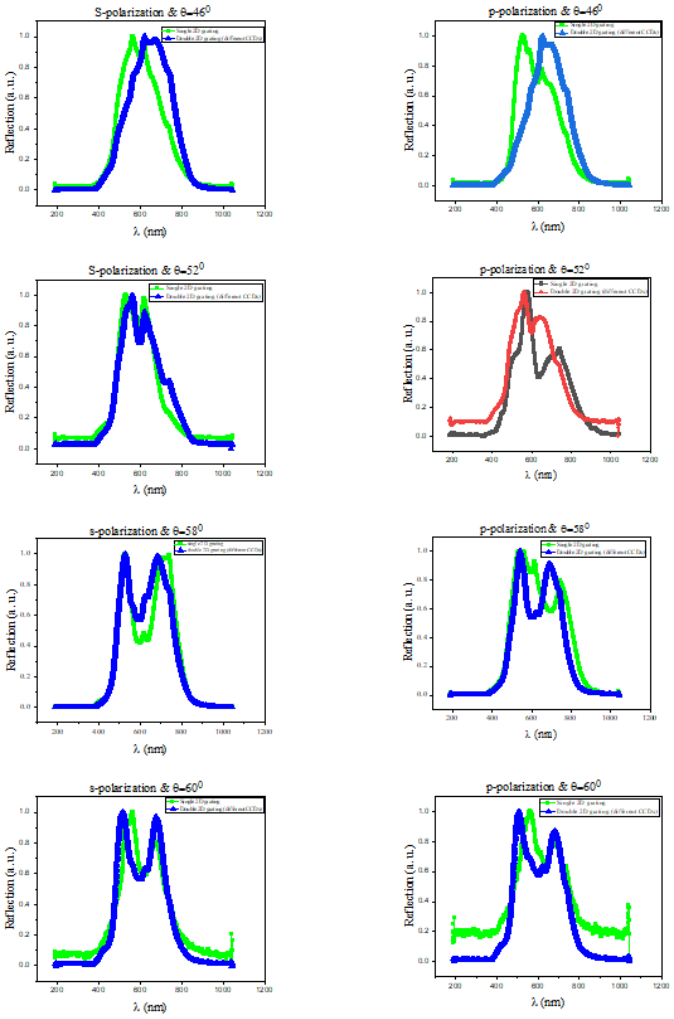

Figure 4. Reflection spectra for the S1 and S2 under different incidence angles.

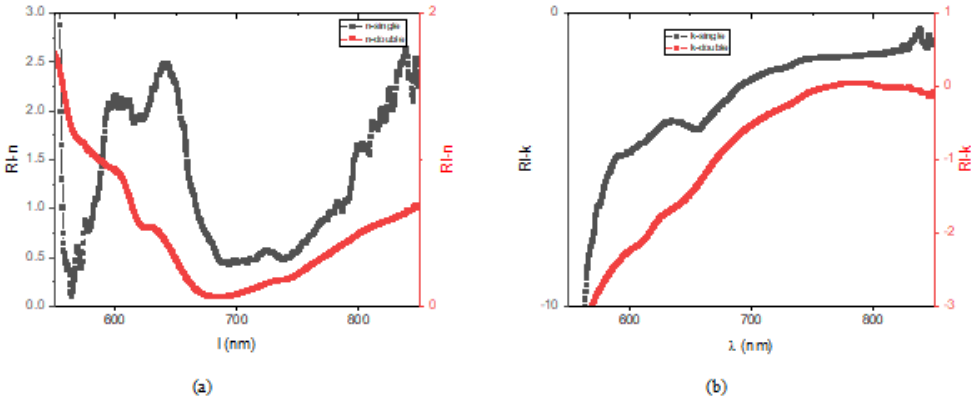

Figure 5. Reflection spectra for the S1 and S2 under different incidence angles.

the first sample, because it consists of one layer, and therefore the absorbance is lower. As for the second sample, the intensity is lower as it has two layers, and therefore the absorbance is higher in this sample. As for diffraction, we notice that the beam width is greater in the second sample since the exposure is larger considering the presence of two grating the refraction of the prepared samples were measured, and the results were as follows. The case of high symmetry that appeared in the previous images, which arose from the presence of a supercell of the prohibited samples, and that the first sample (one side) showed a higher symmetry than (two side) since it causes a higher diffraction condition than the first sample.

In the suggested structures, each TiO_2 unit cell (Fig. 1b) can support an electric (and magnetic) dipole mode. As a consequence, the coupling between electric (as well as magnetic) dipole modes in a periodic arrangement leads to a significant enhancement in the magnitude of the resonance modes, such as the localized surface plasmon resonance (LSPR) in traditional plasmonic nanostructures. The reflection spectra of both samples were measured at different incidence angles of 46°, 52°, 58°, and 60° under s- and p-polarization (Fig. 4). As seen, two distinct resonances were observed in the form of two peaks that correspond to the electric dipole (ED) and magnetic dipole (MD) resonances, respectively. This phenomenon can be explained by the coupling between electric (and magnetic) dipole modes in the fabricated periodic structure. Although electric dipole and magnetic dipole modes appeared under incidence angles of 46° and 52°, stronger resonance occurred at an incidence angle of 58° in which ED and MD resonance modes were separately observed.

The resonance wavelength depends on various parameters such as the geometric dimensions of the structure, the material type, the light polarization, and the incidence angle. For the proposed etalon structure, the location of the resonance dip under p-polarization is shifted toward longer wavelengths at an incidence angle of 58° (Fig. 4).

This red shift can be explained according to the coupling of the dipole moment of each neighboring unit cell. It appears that in larger incidence angles, the greater the separation in the peak, where the clear separation represents the ED on the left and MD on the right, and we notice that the gradient of the increase in the angle begins to appear and become more clear, as we notice its appearance at the 52° and increase at 58° and the most obvious at the angle of 60°. The reason for this separation at these angles may be the fall of the beam by the oblique angle, and it is clear that the fall by the oblique angle leads to the behavior of the metamaterail more clearly.

To gain more insight into the physical reason of the meta-structure of the samples, we calculated the refractive indices of the samples as indicated in Figure 5. Changes in the refractive index within the wavelengths, where we notice the convergence at the wavelength (700 nm) and we notice the difference is large at the wavelength (650 nm), where the single is higher and therefore the linear applications of the double are greater because it has a greater refractive index and thus decreases.

As for the imaginary part of the refractive index, we note an increase in the single within the wavelengths from 550 nm to the end of the visible spectrum, and after that there is a clear reduction. While the double has a different behavior, as there is a decline down to the end of the visible spectrum due to the effect of the meta-structure with a note Single has far lower k-values than double.

4. Conclusion

We noticed through the CCD camera that the intensity is high in the first sample, as it consisted of one layer, and therefore the absorbance is lower. As for the second sample, the intensity was lower because it has two layers, and therefore the absorbance was higher in this sample. Also, from the absorption spectra we noticed through the results, the greater the angle, the greater the separation in the peak, where the clear separation represented the (E.D) on the left and (M.D) on the right, and we noticed that the gradient of the increase in the angle begins to appear and become more clear, as we observed its appearance at the angle 52° and the increase at 58° and the most obvious at the angle 60°. The reason for this separation at these angles may be the fall of the beam by the oblique angle, and it is clear that the fall by the oblique angle leads to the behavior of the metamaterial more clearly.

Ethical approval
This manuscript does not report on or involve the use of any animal or human data or tissue. So the ethical approval is not applicable.

Authors Contributions
All authors contributed equally in design the main sample, measure all the processes and also prepare the text.

Availability of data and materials
Data in this manuscript are available by request from the corresponding author.

Conflict of Interests
The authors declare that they have no known competing financial interests or personal relationships that could have appeared to influence the work reported in this paper.

References

[1] E. Awad. "A novel metamaterial gain-waveguide nanolaser.". *Optics & Laser Technology*, **142**:107202, 2021.

[2] M. Brun, S. Guenneau, and A.B. Movchan. "Achieving control of in-plane elastic waves.". *Applied Physics Letters*, **94**:61903, 2009.

[3] T. Rainsford, S. Mickan, and D. Abbott. "T-ray sensing applications: review of global developments.". *Proc. SPIE. Smart Structures, Devices, and Systems*, **1**:14374107, 2005.

[4] M. G. Cotton. "BOOK: Applied Electromagnetics.". *Technical Progress Report (NITA – ITS)*, **3**, 2003.

[5] A. Kamil Boratay and Ö. Ekmel. "Radiation properties of a split ring resonator and monopole composite.". *Physica Status Solidi B*, **244**:1192, 2007.

[6] J. M. Guerra. "Super-resolution through illumination by diffraction-born evanescent waves.". *Applied Physics Letters*, **66**:3555–3557, 1995.

[7] J. M. Guerra, D. Vezenov, P. Sullivan, W. Haimberger, and L. Walter. "Near-field optical recording without low-flying heads: Integral near-field optical (INFO) media.". *Japanese Journal of Applied Physics*, **41**: 1866, 2002.

[8] S. I. Azzam, K. Chaudhuri, A. Lagutchev, Z. Jacob, Y. L. Kim, V. M. Shalaev, A. Boltasseva, and A. V. Kildishev. "Single and multi-mode directional lasing from arrays of dielectric nanoresonators.". *Laser & Photonics Reviews*, **15**:2000411, 2021.

[9] P. A. Dmitriev, S. V. Makarov, V. A. Milichko, I. S. Mukhin, A. S. Gudovskikh, A. A. Sitnikova, A. K. Samusev, A. E. Krasnok, and P. A. Belov. "Laser fabrication of crystalline silicon nanoresonators from an amorphous film for low-loss all-dielectric nanophotonics.". *Nanoscale*, **8**:5043–5048, 2016.

[10] M. Ghasemi, N. Roostaei, F. Sohrabi, S. M. Hamidi, and P. K. Choudhury. "Biosensing applications of all-dielectric SiO 2-PDMS meta-stadium grating nanocombs.". *Optical Materials Express*, **10**:1018–1033, 2020.

[11] N. Roostaei and S. M. Hamidi. "All-dielectric achiral etalon-based metasurface: Ability for glucose sensing.". *Optics Communications*, **527**:128971, 2023.

[12] C. Gigli, G. Marino, A. Borne, P. Lalanne, and G. Leo. "All-dielectric nanoresonators for χ_2 nonlinear optics.". *Frontiers in Physics*, **7**:221, 2019.

[13] N. Roostaei, N. S. Shnan, and S. M. Hamidi. "Red and blue color production by flexible all-dielectric structure.". *Optik*, **230**:166345, 2021.

[14] N. F. Habubi, R. A. Al-Anssari, and J. A. Abd. "Structural, optical and electrical properties of indium doped cadmium oxide thin films.". *Nano Science & Nano Technology: An Indian Journal*, **7**:172–178, 2013.

[15] N. S. Shnan, S. Sadeghi, M. Farzaneh, S. M. Hamidi, V. I. Belotelov, and A. I. Chernov. "Longitudinal magneto-optical Kerr effect in insulator/metal/insulator grating structure.". *Journal of Superconductivity and Novel Magnetism*, **35**:3397–3401, 2022.